Eur. Phys. J. B **43**, 305–318 (2005)
DOI: 10.1140/epjb/e2005-00058-x

THE EUROPEAN PHYSICAL JOURNAL B

Electrical and magnetic properties of $Gd(Ba_{2-x}La_x)Cu_3O_{7+\delta}$

M. Mirzadeh and M. Akhavan[a]

Magnet Research Laboratory (MRL), Department of Physics, Sharif University of Technology, P.O. Box 11365-9161, Tehran, Iran

Received 14 August 2004 / Received in final form 1st December 2004
Published online 15 March 2005 –

Abstract. We have studied the structural, electrical, and magnetic properties of the normal and superconducting states $Gd(Ba_{2-x}La_x)Cu_3O_{7+\delta}$ [Gd(BaLa)123] samples with $0.0 \leq x \leq 0.8$ prepared by the standard solid-state reaction. XRD characterization shows an orthorhombic-tetragonal structural transition at $x = 0.2$. Iodometric titration analysis shows the oxygen content of the samples increase with the increase of La doping. The resistivity curves show that for $x \leq 0.15$, there is metallic behavior, and for $x \geq 0.2$, there is a gradual insulating transition behavior in the normal state. The metal-insulator and superconductor-insulator transitions occur between $x = 0.35$ and $x = 0.4$. The superconducting transition temperature decreases with the increase of La content as two-step curve. The normal-state resistivity is fitted for two and three dimensional variable range hopping (2D&3D-VRH) and Coulomb gap (CG) regimes, separately. The results show that the dominant mechanism is CG for $x \leq 0.35$, and VRH for $x \geq 0.4$. The pinning energy U, derived from the thermally activated flux creep (TAFC) model and Ambegaokar-Halperin (AH) theory, shows a power-law relation as $U \sim H^{-\beta}$. The critical current density decreases with the increase of La doping and magnetic field. The E-J curves show that the induced electric field increases with the increase of magnetic field and La concentration. The magnetization measurements indicate that the critical penetration fields and magnetic current density decrease with La doping.

PACS. 74.72.Bk Y-based cuprates – 74.25.Ha Magnetic properties – 74.25.Fy Transport properties (electric and thermal conductivity, thermoelectric effects, etc.)

Introduction

The trivalent rare-earth substitution in the high temperature superconductor $YBa_2Cu_3O_{7-\delta}$ (Y123) has long been studied. Replacing Y by different rare-earth elements usually does not affect superconductivity expect for Pr. Suppression of superconductivity by Pr doping in R123 have been investigated intensively. For recent reviews on Pr anomaly in HTSC, see reference [1], and for Pr/Ba site-mixing disorder in R123, see reference [2]. A number of models have been proposed to explain this anomaly. Earlier explanation includes: 1) Hole filling by Pr ions, assumed to have a valance greater than 3+ [3,4]. The hole-filling model was found to be inconsistent with the results of various spectroscopic studies [5,6], which showed a valance close to 3+ for Pr. Also, structural considerations have pointed to trivalent Pr [7]. 2) Magnetic pair breaking by the magnetic moment of Pr [8] was questioned by the fact that other rare earths such as Gd and Sm have 4f moments larger than Pr, but do not suppress superconductivity. 3) As a variation of the hole-filling model, charge redistribution between the CuO_2 planes and the CuO chain layers has later been suggested [9]. 4) The idea that the hybridization of Pr-4f and O-2p orbital in the superconducting CuO_2 plane localizes the holes is considered as the most realistic model to explain the suppression effect due to Pr doping [10].

Recently, superconductivity at about 80 K for Pr123 single crystals, grown by traveling-solvent floating-zone (TSFZ) method, has been reported [11]. The Pr on Ba site mis-substitution is supposed to be responsible for the metal-insulator transition in Pr123. However, the difference between the nonsuperconducting and superconducting Pr123 is not yet clear. To clarify the role Pr plays in R123, in particular to differentiate the effect of Pr at the rare-earth or Ba sites, it is necessary to control not only how much Pr is in the compound, but also the site it occupies. An appropriate means to understand the effect of Pr at Ba site is to study $R(Ba_{2-x}Pr_x)Cu_3O_{7+\delta}$ and compare it with $(R_{1-x}Pr_x)Ba_2Cu_3O_{7+\delta}$ and $R(Ba_{2-x}R'_x)Cu_3O_{7+\delta}$ compounds. The structural study of $Gd(Ba_{2-x}Pr_x)Cu_3O_{7+\delta}$, and comparing it with $(Gd_{1-x}Pr_x)Ba_2Cu_3O_{7+\delta}$ compounds are presented in reference [12].

Also, the electrical properties of high-T_c superconductors, normal state, and superconductor state have been the subject of a great number of research. For promoting

[a] e-mail: akhavan@sharif.edu

Table 1. The values of mass density, oxygen content $(7+\delta)$, onset transition temperature (T_c^{onset}), width of superconducting transition (ΔT_c) and ratio of the resistivity at $T = 300$ K to the resistivity at $T = 100$ K for different amounts of La in Gd(BaLa)123.

x	density (g/cm^3)	$7+\delta$	T_c^{onset} (K)	ΔT_c (K)	ρ_{300}/ρ_{100}
0.0	4.57	6.98	94	5	1.45
0.1	4.75	7.01	90	7	1.50
0.15	5.28	6.95	69	8.5	1.46
0.2	4.81	7.04	62	10	1.20
0.25	4.53	7.08	57	10	1.05
0.3	4.53	7.09	55	14	1.00
0.35	4.59	7.12	47	14	0.95
0.4	4.68	7.13	—	—	0.58
0.5	4.11	7.17	—	—	0.52
0.6	4.52	7.19	—	—	—
0.7	4.72	7.25	—	—	0.03
0.8	4.60	7.4	—	—	0.005

partial application of high-T_c superconductor, it is necessary to improve the flux pinning properties of these materials. Much experimental works have been focused on the relationship between the dissipative flux motion and the flux pinning mechanisms [13–17]. For a detailed understanding of the effects caused by chemical doping and irradiation [18], it is important to regard the underlying microscopic pinning mechanisms.

In single crystals [19] and oriented thin films [20,21], strong magnetic fields are required to show the broadening of transition, while for granular materials, small fields causes more broadening [22,23]. Many groups such as Iwasaki et al. [24], Palstra et al. [25], Batlogg et al. [26], Malozomoff et al. [27], and Griessen [28] have applied the thermally activated flux creep (TAFC) model to describe the broadening of the resistivity near $T_c(\rho = 0)$. At higher temperatures, the flux creep description is only applicable if $U > k_B T$. If the barriers become comparable to thermal energies, the flux flow is more effective in the resistance broadening than the flux creep and the diffusion models; correspondingly, the flux flow is more appropriate than the hopping model for flux creep.

The observed unusual broadening in the resistive transition even for the magnetic field applied parallel to the transition current, has led many researchers to suggest different interpretations for the origin of the broadening. Reasons such as flux line melting [29], flux cutting, and thermally activated phase slip [30] have been proposed.

An alternative approach to the problem of flux line lattice motion in a magnetic field leading to induced dissipation behavior of the high-T_c oxides, has been achieved by applying the AH phase-slip model (AH) [30] to a medium of Josephson weak links, regarded as a single effective junction, as originally suggested by Tinkham and Lobb [31,32]. The results of examination of this model to interpretation of the experimental data [33] show that good agreement exist between the experimental data and the theory.

This investigation is to study the effect of Ba substitution by the rare-earth element La on the electrical and magnetic properties of Gd-based 123 system, and comparison with other rare earths like Pr [33,34] and Nd [35]. We have chosen the 123 solid solution based on Gd with small ionic size relative to the substituted rare earth, so that La to have a greater tendency to substitute for Ba rather than for Gd.

Experimental details

Polycrystalline samples of $Gd(Ba_{2-x}La_x)Cu_3O_{7+\delta}$ [Gd(BaLa)123], with x equals to 0.0, 0.05, 0.1, 0.15, 0.2, 0.25, 0.3, 0.35, 0.4, 0.5, 0.6, 0.7, and 0.8 were synthesized through the standard solid-state reaction route from stoichiometric compound of 3N pure powders of Gd_2O_3, La_2O_3, $BaCO_3$ and CuO. These mixtures were ground and calcined in air at 840 °C for 24 h. The calcinations were repeated twice with intermediate grinding. The compounds were pressed into pellets of 11 mm diameter, and sintered in oxygen atmosphere at 930 °C for 24 h. Then, the samples were cooled to 550 °C, retained there for 4 h, and finally cooled down to room temperature with slow cooling rate of 1 °C/min. The final samples were examined by X-ray diffraction with Cu K_α radiation ($\lambda = 1.5406$ Å) at room temperature. For the resistivity and density measurements, the samples were cut as rectangle with the nominal dimensions $2 \times 3 \times 5 - 10$ mm^3. The resistivity was measured within the temperature range 10–300 K by ac four probe method with the applied current of 5 mA and frequency of 33 Hz. The Cu wires were attached to the sample by silver paste. A Lake Shore-330 temperature controller with a Pt-100 resistor and a GaAs diode was used for measuring and controlling the temperature to within ±10 mK. The oxygen contents of the samples were determined by the iodometic titration technique with the accuracy of ±0.01. Magnetization measurements were carried out on a variable sample magnetometer (PAR-155) under an applied magnetic field of 0–20 kOe.

Results and discussion

Microstructure

The mass density of the samples was calculated from the mass of rectangle samples with accuracy of 10^{-5} g and its volume with accuracy of $10^{-2} \times 10^{-1} \times 10^{-1}$ mm^3. The values of mass density are presented in Table 1. The

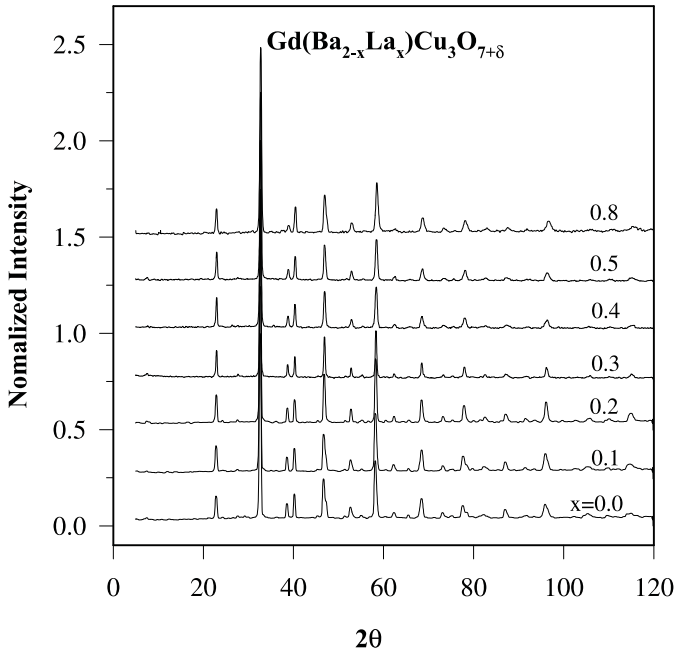

Fig. 1. The observed XRD patterns for $x = 0.0$, 0.1, 0.2, 0.3, 0.4, 0.5, 0.8.

values of the experimental mass density are about 68% of the mass density calculated from the lattice parameters. By La doping, the value of mass density remains nearly unchanged. This is expected because the substitution of La^{3+} with $R_{La^{3+}} = 1.061$ Å and $M_{La} = 138.91$ for Ba^{2+} with $R_{Ba^{2+}} = 1.34$ Å and $M_{Ba} = 137.34$ should not affect the mass density of the samples.

The results of iodometric titration indicate that the value of oxygen content in Gd123 is 6.98, and increases to 7.4 for $x = 0.8$. This increase in the oxygen content with La doping is expected due to substitution of the trivalent La ion for the divalent Ba ion and the charge neutrality requirement. The values of oxygen content for different amounts of La are presented in Table 1. When R^{3+} occupies the Ba^{2+} site, charge balance requires 1/2 oxygen for each R that is incorporating into the structure. In the fully oxygenated orthorhombic structure, the extra oxygen will occupy the anti-chain sites (O5). Therefore, the increase of La doping in the orthorhombic structure causes the increase of occupancy of the O(5) site; the occupancy of O(5) approaches to the O(1) occupancy at $x = 0.2$. In the tetragonal structure ($x \geq 0.2$), the occupancy of O(1) and O(5) persist to be equal. We also calculated the amount of oxygen in the Gd123 sample by using the empirical relation $7 - \delta = 77.78 - 6.153c$ (Å), which was originally derived for pure Y123 [36]. The c lattice parameter was obtained from the Rietveld refinement of XRD pattern. By using the above relation, the obtained oxygen content of Gd123 equals to 6.99, which almost agrees with the experimental value.

Crystal structure

We examined the crystal structure of Gd(BaLa)123 samples by X-ray powder diffraction (XRD). Figure 1 shows the XRD patterns for the samples with $x = 0.0$, 0.1, 0.2, 0.3, 0.4, 0.5, and 0.8. The results indicate that the R123 phase has been formed without considerable impurity phase. The (200) and (020) peaks near $2\theta \approx 47°$ in $x = 0.0$ and 0.1 samples are characteristic of the existence of an orthorhombic phase. So, for $x < 0.2$, an orthorhombic structure with Pmmm symmetry, and for $x \geq 0.2$, a tetragonal structure with P4/mmm symmetry have been used in the Rietveld refinements. In the refinement of the structures, when we used the fixed site occupation factors for atoms in the compound, negative isotropic displacements (B) were found for some atoms. Therefore, we used the occupation factor and isotropic displacements as the variable parameters. The structural parameters for the samples were refined so that the calculated pattern fits the observed one.

Figure 2 shows the observed and the calculated X-ray diffraction patterns for $Gd(Ba_{1.9}La_{0.1})Cu_3O_{7.01}$. The refined parameters of atoms are shown in Table 2. These include lattice parameters (a, b, c), site occupation factor (N), isotropic displacement (B), relative position of atoms in c direction (Z), volume of the unit cell (V), buckling angle (the angle between O(2)-Cu(2)-Cu(2)), the Cu-O bond length (Cu(2)-O(4)), pattern factor of the refinement (R_p), and weighted pattern of the refinement (R_{wp}), which are presented for the following positions of atoms: $Gd(0.5, 0.5, 0.5)$, $Ba/La(0.5, 0.5, Z_{Ba/La})$, $Cu(1)(0.0, 0.0, 0.0)$, $Cu(2)(0.0, 0.0, Z_{Cu(2)})$, $O(1)(0.0, 0.0, 0.5)$, $O(2)(0.5, 0.0, Z_{O(2)})$, $O(3)(0.0, 0.5, Z_{O(3)})$, $O(4)(0.0, 0.0, Z_{O(4)})$ and $O(5)(0.5, 0.0, 0.0)$. For the tetragonal structure ($x \geq 0.2$), we apply $Z_{O(3)} = Z_{O(2)}$ and $N_{O(1)} = N_{O(5)}$.

The lattice parameter a increases and b decreases with the increase of La doping until for $x = 0.2$, for which a is almost equal to b, and for $x > 0.2$, $a = b$, where the tetragonal phase dominates (Fig. 3). This transition is due to the O(5) occupation with appearance of La^{3+} at the Ba^{2+} site. For $x \geq 0.2$, the coexistence of O(1) chain and O(5) anti-chain oxygen makes the a and b directions equivalent, and the tetragonal phase forms. The lattice parameter along the c-axis decreases monotonically (Fig. 3), which is due to substitution of the smaller La^{3+} (1.061 Å) ion at the Ba^{2+} (1.34 Å) site. Thus, we conclude that the doping ions preferentially occupy the Ba sites.

The substitution of La^{3+} for Ba^{2+} induces the inner contact stress around the Ba site. The results of refinements show that the distance between the CuO chain and CuO_2 sheets decreases, which induces the decrease of lattice parameter c and unit cell volume with La doping. The buckling angle of CuO_2 plane decreases as x increases (Tab. 2), resulting in flattening of the CuO_2 planes. As the La doping increases, the Cu-O bond length (Cu(2)-O(4)) becomes shorter by 1.9% from $x = 0.0$ to $x = 0.5$ due to the decrease of the c parameter.

In the R-rich systems, with the increase of doping, decomposition of the perovskite type phase occurs and the impurity phase (i.e., K_2NiF_4 phase) appears in the XRD patterns for $x \geq x_c^{\text{solubility}}$ [37]. The XRD patterns in Figure 1 indicate that the structure for $x = 0.8$ is

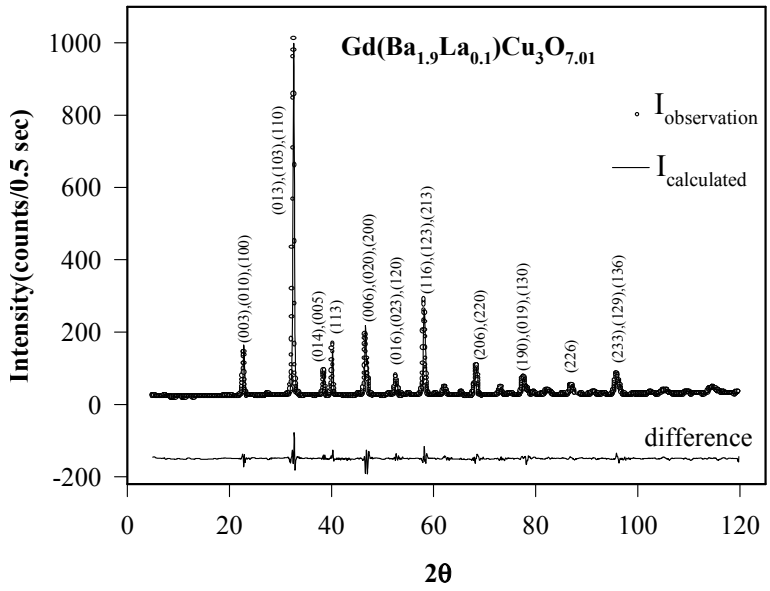

Fig. 2. The observed XRD pattern, the calculated refinement points, and their difference (at the bottom) for $Gd(Ba_{1.9}La_{0.1})Cu_3O_{7.01}$.

Table 2. The results of Rietveld refinement for different amounts of La.

x	0.0	0.1	0.2	0.3	0.4	0.5	0.8
a (Å)	3.855	3.858	3.872	3.874	3.876	3.875	3.867
b (Å)	3.896	3.890	3.875	3.874	3.876	3.875	3.867
c (Å)	11.665	11.662	11.645	11.634	11.585	11.562	11.508
N Gd	0.934	0.939	0.963	0.902	0.927	0.964	0.926
B(Å)	0.959	0.622	0.231	0.634	0.448	0.199	0.457
N Ba	0.973	0.945	0923	0.850	0.801	0.780	0.615
B(Å)	1.59	2.522	4.109	2.247	1.799	1.954	2.867
Z	0.1814	0.1809	0.181	0.181	0.180	0.181	0.178
N La	—	0.066	0.102	0.158	0.224	0.258	0.401
B(Å)	—	2.332	3.919	2.056	1.464	1.765	2.677
N Cu(1)	1.247	1.277	1.136	1.098	1.090	1.024	1.009
B(Å)	7.165	4.72	2.926	2.888	1.219	2.281	3.109
N Cu(2)	0.957	0.928	0.933	0.901	0.909	0.975	0.995
B(Å)	0.678	0.827	1.726	0.898	0.619	0.999	2.152
Z	0.351	0.352	0.355	0.353	0.354	0.352	0.350
N O(1)	0.84	0.576	0.52	0.545	0.565	0.585	0.700
N O(5)	0.14	0.434	0.52	0.545	0.565	0.585	0.700
Z O(2)	0.377	0.378	0.379	0.376	0.376	0.373	0.371
Z O(3)	0.391	0.381	0.379	0.376	0.376	0.373	0.371
Z O(4)	0.154	0.156	0.159	0.158	0.158	0.157	0.161
V (Å^3)	175.19	175.02	174.72	174.60	174.06	173.61	172.08
$\theta_{\mathrm{buckling}}(^\circ)$	8.94	8.93	8.22	7.86	7.46	7.14	7.12
$Cu_{(2)}$-$O_{(4)}$ Å	2.298	2.286	2.282	2.268	2.270	2.254	2.175
R_p (%)	7.55	7.36	8.04	11.1	9.98	10.14	6.16
R_{wp} (%)	9.82	9.58	12.18	14.3	12.72	13.09	7.90

single phase 123, and there is no impurity phase like K_2NiF_4 type in the sample. Thus, the solubility limit in the Gd(BaLa)123 system should be higher than 0.8. The solubility of R in $R_{1+x}Ba_{2-x}Cu_3O_y$ depends on the ionic radius of R^{3+}. Goodenough et al. [38] have used a geometrical parameter, the tolerance factor, as a numerical criterion of the stability of a perovskite. The tolerance factor for ABO_3 perovskite structure is defined as:

$$t = \frac{r_A + r_O}{\sqrt{2}(r_B + r_O)}, \quad (1)$$

where, r_A, r_B, and r_O are the radii of the A, B, and oxygen ions [38]. The perovskite structure forms with $0.8 \leq t \leq 1.0$. Since the R123 structure is a distorted layer perovskite structure, the tolerance factor should still be valid to describe the stability of the R123 structure. From the point of view of the average structure, by using equation (1), the tolerance factor for R(BaR′)123 can be written as:

$$t = \frac{r_R/3 + (2-x)r_{Ba}/3 + x r_{R'}/3 + r_O}{\sqrt{2}(r_{Cu} + r_O)}, \quad (2)$$

where, r_R, $r_{R'}$, r_{Ba}, and r_{Cu} represent the average radii of ions occupying the R, R′, Ba, and Cu sites, respectively, for cations doped R123 system. R′ is the rare earth ion that substitutes at the Ba site. Lide and Frederkee [39] and Tang and Gao [40] have reported the calculated tolerance factors for R123 and R-rich R123 systems. The R123 structure can only exist for a certain value of R^{3+} substitution for Ba^{2+}. The solubility of R ions at the Ba site depends on the size of the rare earth ion. The larger rare earth ion has larger solubility. Cava et al. [41] have successfully synthesized the Y(BaLa)123 compound with $x \leq 1.0$. The critical tolerance factor for this system is obtained $t_c \sim 0.8329$. Here, to calculate the tolerance factor, we have taken the ionic radii of R^{3+}, Ba^{2+}, Cu^{2+}, and O^{2-} used in reference [39]. The solubility limit can be determined by the critical tolerance factor in the similar compound that has been obtained from experiment. If we assume the critical tolerance factors in Gd(BaLa)123 and Y(BaLa)123 to be similar, then we could estimate the solubility limit of La in this compound by using equation (2). By assuming $t_c \sim 0.8329$, we obtained the critical solubility limit for our system, $x_c^{\text{solubility}} = 1.14$. This gives us assurance that the highest $x = 0.8$ sample in our study is below the solubility limit of the Gd(BaLa)123 system.

Normal state resistivity

Figure 4 shows the resistivity versus temperature for different amounts of La doping. The resistivity at the room temperature increases with the increase of La doping. The temperature dependence of resistivity proceeds linearly down to 125 K for Gd123. The range of temperature in which the resistivity behaves nearly linear, becomes shorter with the increase of La doping, as the linear dependence of resistivity at $x = 0.35$ is observed only in the temperatures higher than 190 K. At the room temperature,

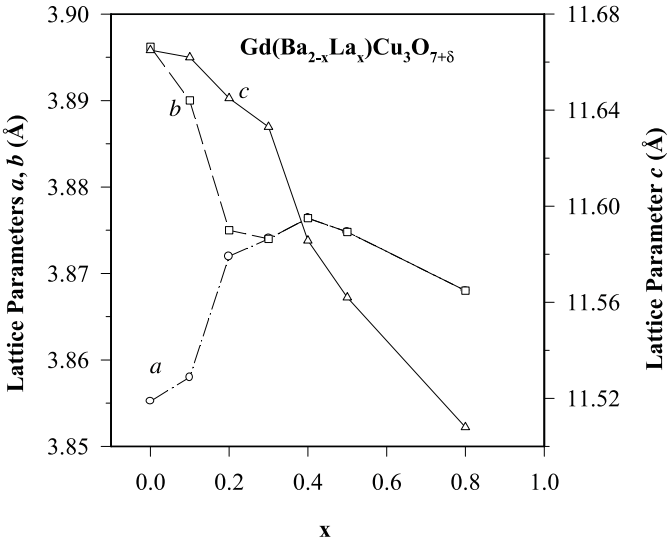

Fig. 3. The lattice parameters vs. amount of La doping x. The lines are guides to the eye.

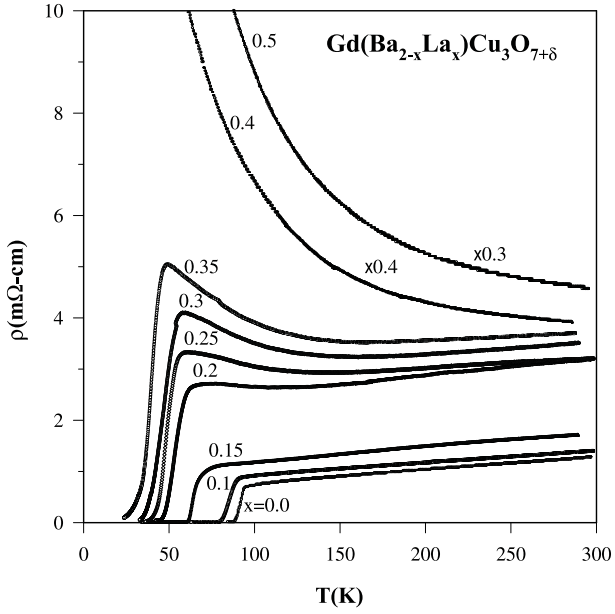

Fig. 4. The resistivity vs. temperature for different amounts of La doping x.

with the increase of La content x, the resistivity increases, and the slope of resistivity ($d\rho/dT$) decreases. Further, as temperature is lowered, the rate of increase in resistivity increases with x. The obtained values of ρ_{300}/ρ_{100} for different x are presented in Table 1. This ratio decreases with the increase of La, and for the insulating samples this value becomes very small.

The $\rho(T)$ curves for the $x \geq 0.2$ samples (Fig. 4) shows a deviation from the general trend. In these samples the behavior of resistivity with the decrease of temperature changes from metallic to semiconducting, and $\rho(T)$ curves show a minimum at T_{min}, and after passing through a maximum, the superconducting transition occurs. The value of T_{min} increases with the increase of La content,

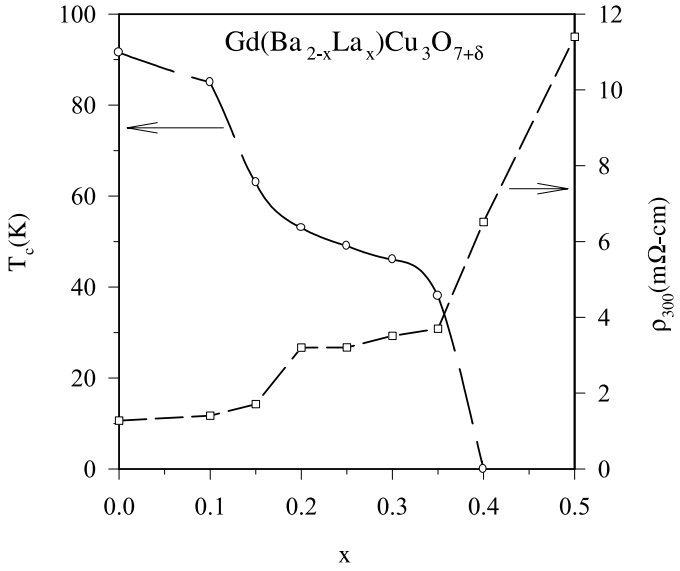

Fig. 5. The T_c and ρ_{300} vs. the La content, x.

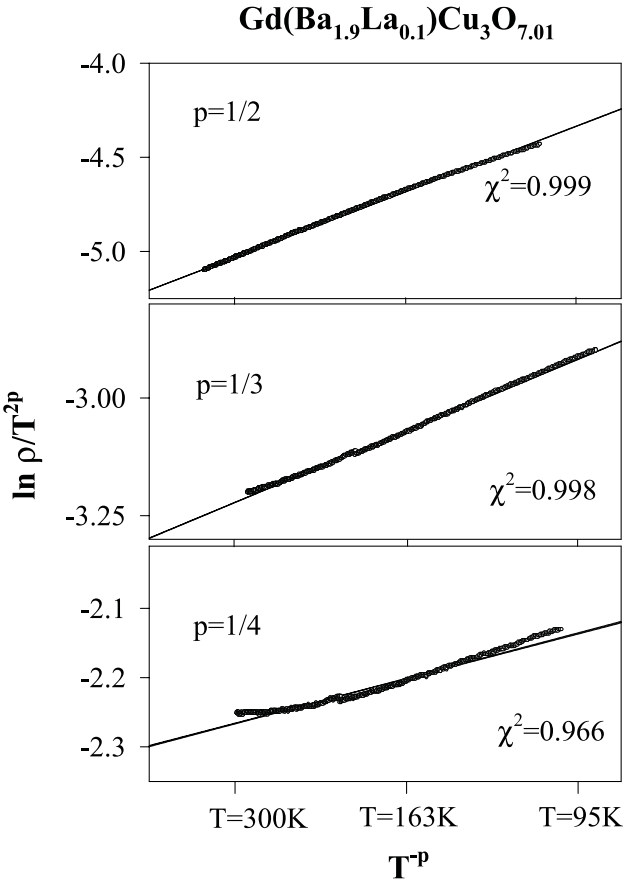

Fig. 6. The linear fittings of $\ln\rho/T^{2p}$ vs. $1/T^p$ with $p = 1/2$, 1/3, and 1/4 for $Gd(Ba_{1.9}La_{0.1})Cu_3O_{7.01}$.

and when T_{min} is quite high, ρ(T) just shows a semiconducting behavior in the temperature range 20–300 K. It is observed that the minimum of resistivity in the normal state for $x = 0.4$ occurs for $T > 300$ K. The metallic behavior in the normal state remains up to $x = 0.35$, and there is an insulator-like behavior for $x \geq 0.4$ in the Gd(BaLa)123 system. The metal-insulator transition, $x_c^{\rm MIT}$ is between $x = 0.35$ and $x = 0.4$. The sample of $x = 0.35$ is the last superconductor sample, and the superconductor-insulator transition, $x_c^{\rm SIT}$, occurs between $x = 0.35$ and $x = 0.4$. The value of $x_c^{\rm SIT}$ for Gd(BaLa)123 is almost equal to its value for Gd(BaPr)123, but its $x_c^{\rm MIT}$ value is less than the one for Gd(BaPr)123 compound [42]. In our other study, we found that for the Gd(BaNd)123 system $x_c^{\rm MIT} = 0.2$ and $x_c^{\rm SIT}$ is between 0.35 and 0.4 [35]. It seems that different effects due to the substitution of La, Nd, and Pr doping appear in the MIT phenomenon.

Figure 5 shows the dependence of the room temperature resistivity upon La content x. The room temperature resistivity increases with La doping. The small amount of doping has no appreciable effect on the electrical properties, and the room temperature resistivity remains unchanged. There is a two-step variation in ρ_{300} with La content in Gd(BaLa)123. As can be seen in Figure 5, the variation of ρ_{300} for $x \leq 0.15$ and for $0.2 \leq x \leq 0.35$ is small. It is noticeable that the samples with $x = 0.0-0.15$ show metallic behavior for $T > T_c$, and for the samples with $x = 0.2-0.35$ there is T_{min} in the normal state resistivity. As will be considered later, the magnetic behaviors in these samples are similar as well. It seems that a correlation exists between the magnetic properties in the superconducting transition and the normal state properties.

In different reports, the hopping conduction between the localized states has been used for the normal state of high-T_c superconductors [43] and semiconductors [44,45]. We have studied the normal-state resistivity of the Gd(BaLa)123 samples within the variable range hopping (VRH) and Coulomb gap (CG) models. In the hopping conduction, the temperature dependence of resistivity is expressed as following [44]:

$$\rho(T) = \rho_0(T) \left(\frac{T}{T_0}\right)^{2p} \exp\left(\frac{T_0}{T}\right)^p. \qquad (3)$$

For an energy-independent DOS, this leads to a Mott-Davis transition [46] VRH case of $p = 1/3$ in two dimensions, and $p = 1/4$ in three dimensions. Shklovskii and Efros [44] have analyzed the case of low carrier concentration in doped semiconductors, where electrons interact via the unscreened Coulomb potential. This leads to a gap in the DOS that is pinned to E_F. This leads to the same exponent $p = 1/2$ in equation (3).

We have fitted the $\ln(\rho/T^{2p})$ vs. $1/T^p$ curve by a linear function for different values of p. This fitting has been applied in the temperature interval between the transition temperature to the room temperature for the superconducting samples, and $T > 50$ K for the insulating samples. Figure 6 shows a typical curve for $Gd(Ba_{1.9}La_{0.1})Cu_3O_{7.01}$. The ρ(T) of $x \leq 0.35$ samples could be fitted better with $p = 1/2$ -CG is the dominant conduction regime. For $x \geq 0.4$, the conduction mechanism is VRH, and the 3D-VRH is dominant. There is a crossover from CG to VRH with the increase of x. DOS at E_F for the superconducting samples is nonzero and for the insulating samples is zero. The derived parameters T_0

Table 3. The derived parameter T_0 and ρ_0, the quality of fit χ^2, and the obtained T_{min} from theory and experiment.

	x	T_0	ρ_0	χ^2	T_{min} (K)	T_{min}^{exp} (K)
CG regime $p = 1/2$	0.00	186	0.44	0.998	46	—
	0.10	261	0.63	0.998	65	—
	0.15	262	0.67	0.998	65	—
	0.20	429	1.36	0.999	107	118
	0.25	577	0.84	0.999	144	145
	0.30	647	1.76	0.999	161	158
	0.35	686	1.91	0.999	171	170
3D-VRH $p = 1/4$	0.40	51153	2.13	0.996	43014	—
	0.50	76667	3.15	0.997	64469	—
	0.70	7407699	0.09	0.998	6229107	—
	0.80	6104782	0.37	0.998	5133489	—

and ρ_0, and the quality of fit χ^2 for $p = 1/2$ at $x \leq 0.35$ and for $p = 1/4$ at $x \geq 0.4$ are presented in Table 3. By setting the derivative of equation (3) equal to zero, a minimum occurs at $T_{min} = T_0/2^{1/p}$. We calculated T_{min} from the above equation, and obtained the minimum from the experimental data in the normal-state resistivity (Tab. 3). The results indicate that the experimental T_{min} is about equal to its theoretical value, thus good agreement exists between the experimental data and the fitting of CG regime for these samples.

There are different reports on the conduction mechanism of HTSCs in the literature. For polycrystalline GdPr-123 samples, the conduction mechanism in the normal state for $x \geq 0.35$ is 3D-VRH and for $x < 0.35$ is CG mechanism [47]. In $Pr_{1+x}Ba_{2-x}Cu_3O_{7+\delta}$ with 20 K $< T <$ 300 K, the 3D-VRH [48], and in Gd(BaPr)123 system, 2D-VRH [42] are the dominant conduction mechanisms. The conduction mechanism for Tm(BaPr)123 has been reported to be CG for $x < x_c^{\rm MIT}$, and 2D-VRH for $x_c^{\rm MIT} \leq x \leq x_c^{\rm SIT}$, and 3D-VRH for $x > x_c^{\rm SIT}$ [49]. So, CG, 2D-VRH, and 3D-VRH have been reported as conduction mechanisms for normal state resistivity of different HTSCs. The normal state resistivity is highly affected by the different sample preparation conditions like oxygen content. Thus, such disagreements between different reports are expected.

Superconducting and magnetic properties

As can be seen in Figure 4, the resistivity curves indicate that the transition temperature T_c (the temperature at 50% of the resistive transition) decreases and the transition width ΔT_c (the temperature difference between 90% and 10% of resistance at transition) increases with the increase of La doping. Figure 5 shows the dependence of T_c upon La content x. T_c remains unchanged with small value of La content, while more increase in doping causes the decrease of T_c. There is a two-step variation of transition temperature with La content: The first step at $x = 0.0 - 0.1$, and the second step at $0.2 \leq x \leq 0.35$. This plateau variation is also observed in the ρ_{300} vs. x. This is similar to the dependence of T_c upon oxygen content in the Y123 system [50]. The two-step $T_c(x)$ might be

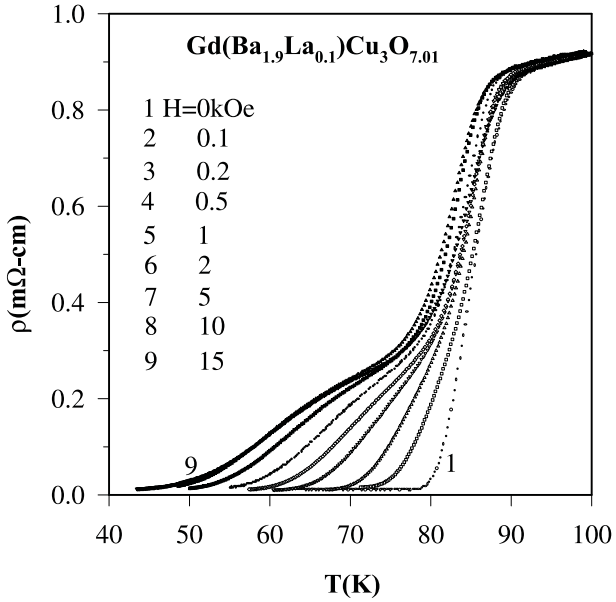

Fig. 7. The broadening of $\rho(T)$ with magnetic field for $Gd(Ba_{1.9}La_{0.1})Cu_3O_{7.01}$.

an indication of the existence of two phases of superconductivity or two levels for hole separated by a small energy interval. With the placement of extra oxygen at the chain site, the trap energy for holes is lowered as one level crosses the Fermi level. With further lowering of the hole trap energy, the second trap level crosses the Fermi level and the second fall take place. It seems that the oxygen content, oxygen ordering, and charge transfer due to the difference in the valances of La^{3+} and Ba^{2+} ions may be the key factors to the superconductivity of Gd(BaLa)123. The transition width, ΔT_c, increases from 5 K in Gd123 to 14 K at $x = 0.35$ (Tab. 1). The large transition widths may result from inhomogeneity of the samples due to La doping, and/or inhomogeneous distribution of La and oxygen, or coexistence of orthorhombic and tetragonal phases, or combination of the above.

We have measured the resistive transition under magnetic field perpendicular to the current and surface of the samples. Figure 7 shows a typical broadening of the resistivity for different applied magnetic field in $Gd(Ba_{1.9}La_{0.1})Cu_3O_{7.01}$ compound. The transition in zero magnetic field is sharp, but broadens considerably upon applying a magnetic field. The normal state resistivity remains unchanged and the onset transition temperature, $T_c^{\rm on}$, remains almost constant with the increase of applied magnetic field. As can been seen in Figure 7, the resistive transition shows two distinct parts, a steep part in the onset of the superconducting transition region, and a tail part at a lower temperature. The steep part is less sensitive to the applied magnetic field due to the strong intragrain pinning energy not allowing any vortex motion. With the increase of doping, the sensitivity of the steep part on the magnetic field increases. The tail part, which depends on the weak links between the grains [51], is extremely sensitive to the magnetic field and moves to lower

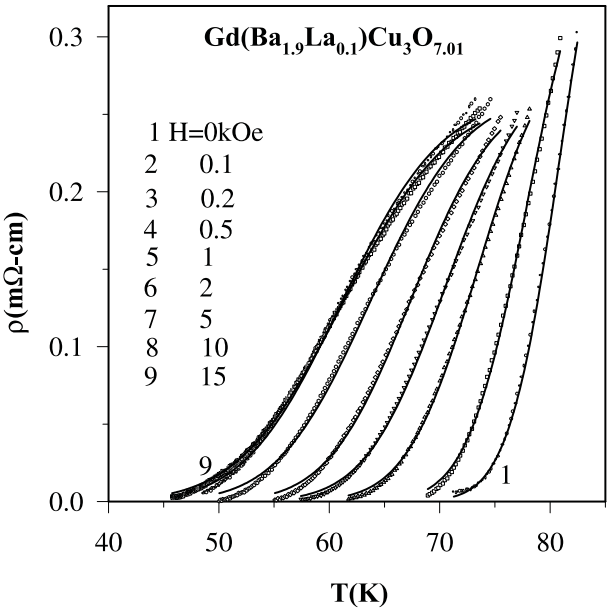

Fig. 8. The $\rho(T)$ broadening at different magnetic fields for $x = 0.1$, fitted with the AH theory.

temperatures with the increase of magnetic field. These two parts are separated from each other at the branching point. With the increase of the amount of La, the distinction between the corresponding two parts becomes less pronounced. It should be noted that the behavior of magnetoresistance curves are affected by the sample characteristics in the intergrain regions such as oxygen content, quality of weak links, and the homogeneity.

To establish the resistive broadening behavior in the Gd(BaLa)123 system, we have used the AH and TAFC models. Near the transition temperature, thermal fluctuations can disrupt the coupling of the phase of the order parameter of the two superconductors forming a Josephson junction. When k_BT becomes comparable with the Josephson coupling energy, $\hbar I_c/e$ (I_c is the maximum Josephson current at temperature T in the absence of noise), the resistivity in the limit of low bias current, $I \ll I_c(T)$ is given by [30]

$$\rho = \rho_n \left[I_0 \left(\frac{\gamma}{2} \right) \right]^{-2}$$
$$\gamma = C(H) \left(1 - \frac{T}{T_c} \right)^q, \qquad (4)$$

where, I_0 is the modified Bessel function, ρ_n is the average normal state resistivity of the junction, and γ is the normalized barrier height for thermally activated phase slip (TAPS). The amounts of reported q are 1.53–2.8 [52].

The experimental data from the branching point were fitted to the AH phase slip model (Eq. (4)) with four fitting parameters, ρ_n, T_c, C, and q. To fit the data, we assumed that C is a magnetic field dependent parameter. So, we determined the variation of C and q with magnetic field and La doping. Figure 8 shows the experimental magnetoresistance data and the fitted curves to the AH model

Table 4. The derived n factor and χ^2 from the AH theory, and β factor and χ^2 from TAFC model for different amounts of La doping.

	$C(H) \sim H^{-n}$		$U_0(H) \sim H^{-\beta}$	
x	n	χ^2	β	χ^2
0.0	0.27	0.978	0.55	0.986
0.1	0.26	0.963	0.47	0.982
0.15	0.19	0.953	0.47	0.988
0.2	0.35	0.985	0.55	0.998
0.25	0.46	0.979	0.67	0.987

for $Gd(Ba_{1.9}La_{0.1})Cu_3O_{7.01}$. In the fitting process, the obtained T_c value is close to T_c^{on}, which remains almost unaffected under the applied magnetic field. Thus, we have omitted it from the fitting parameters. The results of the fitting procedure show good agreement between the experimental curves and the AH model except for the low temperature region near $T_c(\rho = 0)$, which requires an alternative explanation. In this region, the TAFC model is the preferable regime. The results of fitting show that the obtained value of ρ_n remains nearly constant with the increase of applied magnetic field; it is close to the value of resistivity at the branching point of the magnetoresistance curves.

The $C(H)$ parameter versus magnetic field for different amount of La in Gd(BaLa)123 compounds are shown in Figure 9. The $C(H)$ parameter decreases with the increase of La doping. This indicates that the coupling energy between the Josephson vortices decreases with the increase of La content. Also, it is evident that $C(H)$ decreases with the increase of applied magnetic field [28]. In order to examine the magnetic field dependence of $C(H)$, we have plotted log$C$-log$H$ for all the samples. The values of $C(H)$ can be fitted to a H^{-n} power-law relation. The derived amounts of n are presented in Table 4. The value of n are found to be $n = 0.27$, 0.26, 0.19, 0.35, 0.44 for $x = 0.0$, 0.1, 0.15, 0.2, 0.25, respectively. For $x = 0.25$, with the increase of magnetic field, the measurable broadening region for the measured temperatures is very limited, and the fitting of the experimental curves to the AH curve becomes improper. Therefore, we have not considered the $H > 2$ kOe values for calculating the power factor n.

The power-law dependence of $C(H)$ with H is also reported by others [21,23,32,51,53,54]. In different studies, different values for power factor n have been obtained. Kim et al. [21] for Y123 thin films have derived $n = 0.73$ in fields up to 100 kOe. In $Bi_2Sr_2CaCu_2O_{8+\delta}$ single crystal with field up to 55 kOe [55], and in granular Y123 with fields up to 1 kOe [51] and 75 Oe [53], n is reported equal to 0.5. In granular Ca-doped GdPr123 with magnetic fields up to 17 kOe, the value of n has been reported about 0.3 [54], and in Tm(BaPr)123, the value of n increases from 0.15 to 0.3 with the increase of Pr doping [49]. In GdPrBaCa1113 system, n decreases from 0.86 to 0.25 with the increase of Pr doping for magnetic fields up to 2 kOe [56], and in Nd(BaPr)123, the obtained n is about 0.1 for 0.5 kOe $< H \leq 15$ kOe [57]. The above reports indicate that the value of n depends on the range

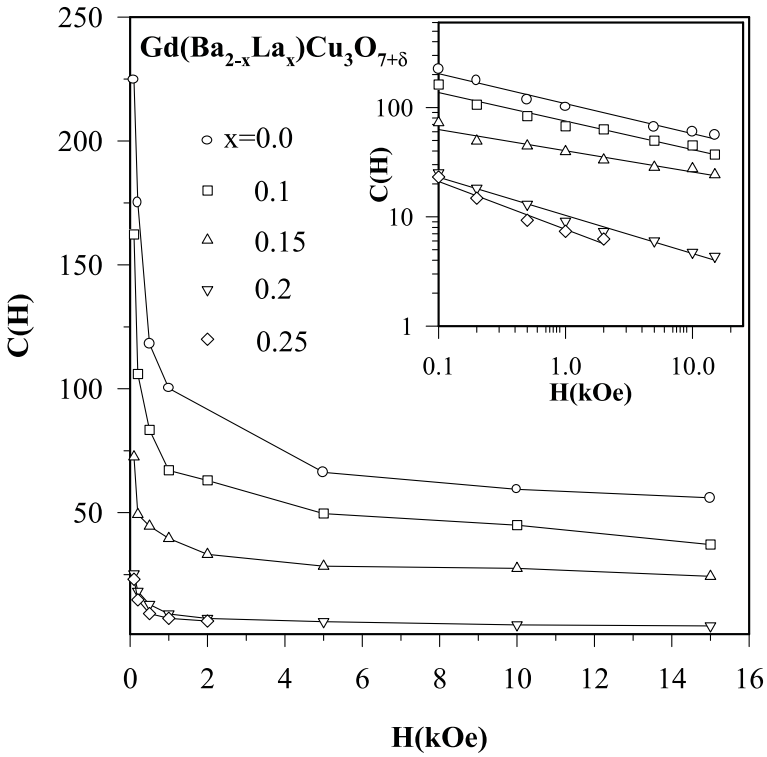

Fig. 9. The $C(H)$ parameter for different magnetic fields and La doping in Gd(BaLa)123. The inset is the log-log plot with linear fittings.

of the applied magnetic field; for larger magnetic fields, n is less than its value for the smaller magnetic fields. The reported values of power factor n is very disperse, because the magnetic variation of $C(H)$ depends on the size and orientation of the weak link Josephson junctions, which are determined by the sample microstructure.

Figure 10 shows the q parameter for different amounts of applied magnetic field and different La contents. With the increase of magnetic field, for $x = 0.0$, 0.1, 0.15 samples, q begins from the value about 1.5 and increases. For $x = 0.2$, this parameter deceases from 2 to about 1.25. For $x = 0.25$, the variation of q is small in the range of magnetic field $H \leq 2$ kOe. Similar behavior has been reported for Gd(BaPr)123 [33]. In both systems, for small amount of doping of Pr or La at Ba site, q increases with H; for larger amounts of doping, q decreases. It is noteworthy that $x_c^q = 0.2$ for which the behavior of q changes –the sample with the lowest x showing a minimum in its normal state resistivity– corresponds to the metal-insulator transition in the normal state. In addition, in the Gd(BaPr)123 system, the value of x_c^q is 0.15 [33], and it seems that it is also the sample with the lowest x showing a minimum in the normal state resistivity. This conclusion indicates that MIT plays an important role in relation with the mixed and normal state phases.

From the AH phase slip theory, the parameter $C(H)$, which is proportional to the activation energy at temperature close to T_c, is given by [51]:

$$C = \frac{J_c(0)\hbar a^2}{ek_B T_c}, \qquad (5)$$

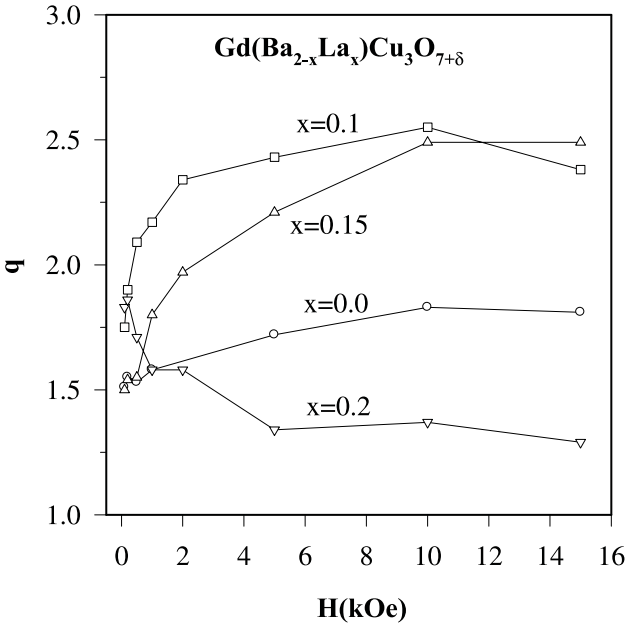

Fig. 10. The exponent q vs. H for different amounts of La doping x.

where, $J_c(0)$ is the critical current at zero temperature, and a is the average grain size. The average grain size in our samples obtained by SEM is about 1 μm. By using equation (5), we estimated the value of $J_c(0)$ for different amounts of La in various magnetic fields. Figure 11 shows

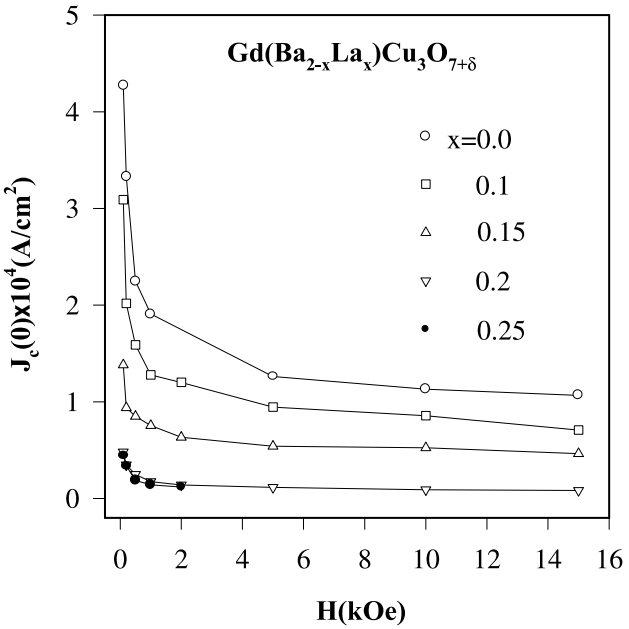

Fig. 11. The critical current density at zero temperature vs. magnetic field for different amounts of La doping. The lines are guides to the eye.

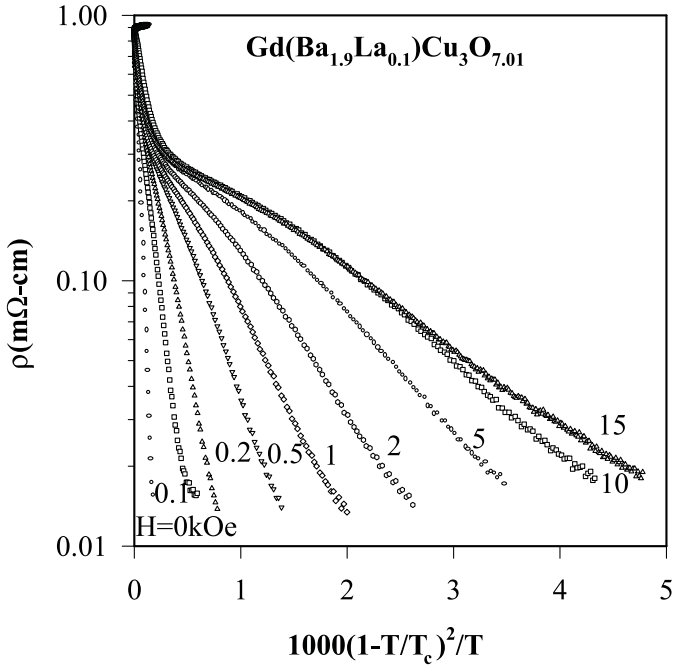

Fig. 12. The $\ln\rho - (1 - T/T_c)^2/T$ plot for different magnetic fields in $Gd(Ba_{1.9}La_{0.1})Cu_3O_{7.01}$.

that critical current in the grain boundaries significantly decreases as La concentration is increased, which in turn, is the evidence of sensitivity of a single junction between the superconducting grains to the applied magnetic field. The decrease of $J_c(0)$ with doping has been observed in similar compounds [33,49,56,57]. The decrease of $J_c(0)$ with the increase of La content indicates that La ions act as weak link.

We have used the TAFC model to study the broadening of the resistivity at the region near $T_c(\rho = 0)$. Many previous studies [19,13–17,52,58] suggest that the thermally activated resistivity in the cuprate superconductors can be characterized in terms of a single activation energy, U, which is the necessary activation or pinning energy to move the vortex, and depends on the temperature and applied magnetic field, such that:

$$\rho(T, H) = \rho_0 \exp\left(-\frac{U(T, H)}{k_B T}\right). \quad (6)$$

In some reports the obtained pinning energy is only magnetic field dependent with a linear behavior in $\ln\rho$-$1/T$, the Arrhenius plot [19]. We have plotted the Arrhenius plot of resistivity at various magnetic fields for different amounts of La doping in a semilog scale. The details of this investigation are presented in reference [59]. The $1/T$ dependence of $\log\rho$ does not show a good linear behavior in the tail part of the resistivity as predicted by Palstra et al. [19]. This indicates that the temperature dependence of activation energy is considerable. The temperature dependence of activation energy is assumed to be $U(T, H) = U_0(H)(1 - T/T_c)^\alpha$, where U_0 is the unperturbed pinning energy at absolute 0 K, with $\alpha = 1.5$ [60–63], 2 [63,64], 1.0 [32,65] for the high temperature superconducting materials. In general, $\alpha = 1.5$ is considered for 3D behavior and $\alpha = 2$ for 2D behavior of HTSCs [66].

The linear fitting of $\ln\rho$-$(1 - T/T_c)^\alpha/T$ curves for the tail part with different values of α, and various amounts of doping, indicates that $\alpha = 2$ is the best power-factor for the pinning energy, which was taken as the optimum value for all samples. We plotted the Arrhenius plot of resistivity with $\alpha = 2$ for different amounts of doping. Figure 12 shows typical curves of $\ln\rho$-$(1 - T/T_c)^2/T$ for $Gd(Ba_{1.9}La_{0.1})Cu_3O_{7.01}$ for different magnetic fields. The slope of the linear data in the tail part of these curves gives the activation energy $U(H)$ for different magnetic fields. The value of $U(H)$ decreases as the magnetic field increases. The pre-exponential factor, ρ_0, is field independent and almost constant, equal to the resistivity value of the branching point of $\rho(T, H)$ curves.

The $U(H)$ for different amount of La doping is presented in Figure 13. The inset shows the $\log U$-$\log H$ for different amounts of dopings, and their linear fittings. The value of $U(H)$ significantly decreases for each applied magnetic field as the La concentration is increased in Gd123. It should be noted that because of the $(1 - T/T_c)^2$ factor, the value of pinning energy is considerably smaller than the value of $U(H)$. This is expected as our results show the decrease of weak link between the grains with the increase of La content.

The decrease of pinning energy with the increase of applied magnetic field can be scaled with a power-law relation ($U \sim H^{-\beta}$). This is also reported for YPr123 [67], GdPr123 [18], epitaxial thin film Y123 [68], and Gd123 [66]. In addition, for Pr doping, the decrease of pinning energy as a power relation has been reported for Nd(BaPr)123 [57] and Gd(BaPr)123 [34]. The values

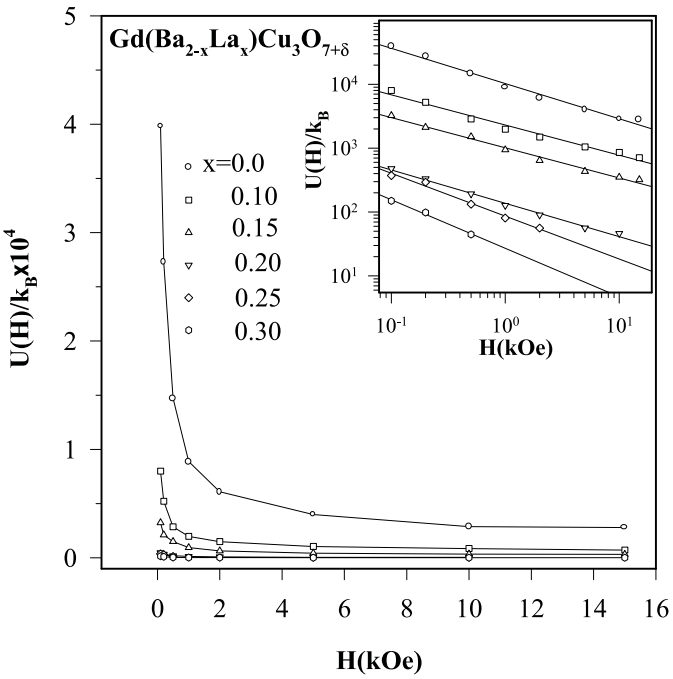

Fig. 13. $U(H)$ vs. H for different magnetic fields and La doping in Gd(BaLa)123. The inset is the log-log plot with linear fittings.

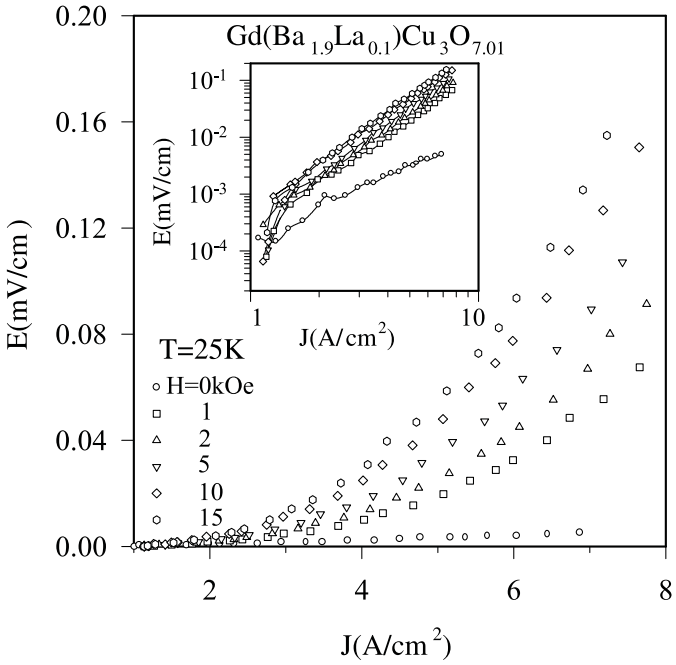

Fig. 14. E-J curves for different magnetic fields perpendicular to the current at $x = 0.1$. The inset is the log-log plot.

of β and the quality of fit, χ^2 for different amounts of La doping are presented in Table 4. For Gd123, the value of β is 0.55, and remains almost unchanged up to $x = 0.15$ for La doping. This is in agreement with the report on GdPr-123 system with small amount of Pr [69]. The value of β in some reports has been derived equal to 0.35 for GdPrCa-123 [54], 0.5 for Y123 [19,53], and 0.5 for Gd123 at $H < 1$ T [66]. Since the resistive tail moves to temperatures lower than the temperature limit accessible for some measurements, it was not possible to determine the zero resistive-state temperature T_{c0} of samples with $x \geq 0.2$ for some values of the applied magnetic field. In these samples, the TAFC model has not been applied for all magnetic fields.

We have calculated the value of the temperature dependent pinning energy $U(H)(1-T/T_c)^2$ at different magnetic fields for different samples. Comparison between the thermal energy and the pinning energy indicates that for the $x \geq 0.2$ samples the TAFC model is not applicable for full range of magnetic field. The thermal energy is greater than the pinning energy at $x = 0.2$ for $H \geq 10$ kOe, at $x = 0.25$ for $H > 5$ kOe, and at $x = 0.3$ for $H > 0.5$ kOe, so explaining the broadening in these regions by the TAFC model is not valid. The value of β in the validity region at $x = 0.20$ equals to 0.55 with $\chi^2 = 0.998$, and at $x = 0.25$ equals to 0.67 with $\chi^2 = 0.986$. These results indicate that the value of β increases with increase of doping $x \geq 0.2$. This is also reported for the high Pr content in Gd(BaPr)123 compound [34]. Hence, the magnetic properties of samples are different for small and large amounts of La doping. The derived value of β for $x \leq 0.15$ is independent of the La content.

I-V Characteristics

The current-voltage characteristics were measured with the magnetic field perpendicular to the current at the low temperatures available for the experiment. We have calculated the electrical field and current density. Figure 14 shows the E-J curve for $Gd(Ba_{1.9}La_{0.1})Cu_3O_{7.01}$ at $T = 25$ K. For the current density less than 2 A/cm^2, the induced voltage is nearly zero. With the increase of current, the observed electric field increases nonlinearly. In the inset to Figure 14, the electric field versus current density in a log-log scale exhibits negative curvature. Such a negative curvature in the log$E$-log$V$ plot occurs only when the resistance is saturating to the normal state value near J_c. This can be shown for the Josephson junction, and must be true for the flux creep. The Anderson-Kim model [70] ignores the normal-state limit of resistance, and predicts only an exponential increase of E with J. This model assumes that the dependence of activation energy to the current at high-current limit is linear, $U = U_0(1 - J/J_c)$. Then, the electric field increases exponentially with the increase of current density. The same current dependence of U has been observed in Y123 epitaxial films [71].

For high current densities, Zeldov et al. [72] have reported the logarithmic current dependence for activation energy, $U = U_0 \ln(J/J_0)$. By assuming the logarithmic dependence of the activation energy, and that the hopping rate of flux lines is $\nu = \nu_0 \exp(-U/k_BT)$, the electric field increases with current as a power-law relation. In our samples, the linear behavior in the log$E$-log$J$ plot at high current shows that the dependence of the activation energy to current is logarithmic. As can be seen in Figure 14, the induced electric field increases with the increase of applied magnetic field, which is due to the increase of the Lorentz

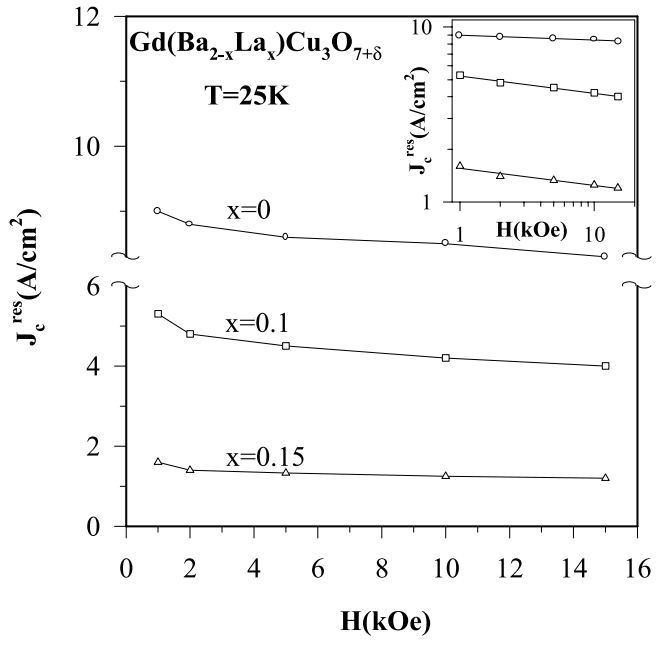

Fig. 15. The derived J_c^{res} from the E-J curves vs. magnetic field for different amounts of La doping. The inset is the log-log plot with linear fittings.

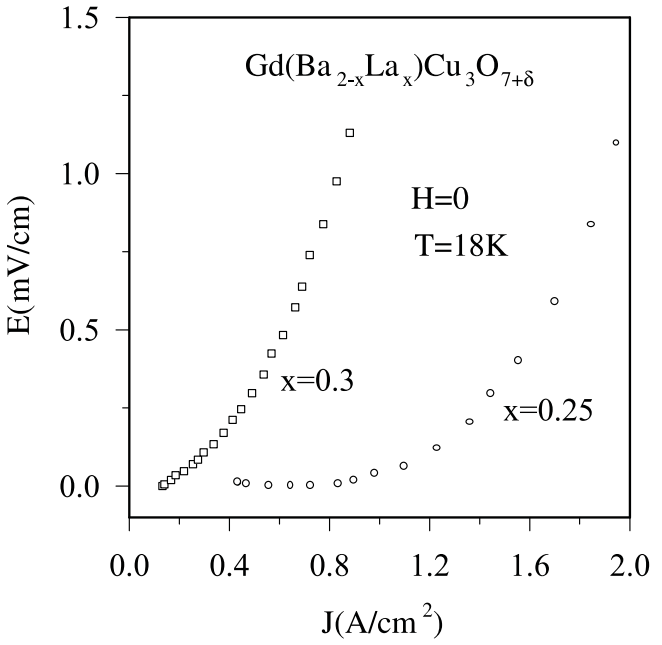

Fig. 16. E-J curves for $x = 0.25$ and 0.3 with zero magnetic field.

force. We chose the crossing of the tangent at the tail end of E-J curves as the resistive critical current J_c^{res}, and obtained the values of J_c^{res} with the applied magnetic field and La doping. Figure 15 shows that J_c^{res} decreases with magnetic field as a power-law relation. The power factor equals to -0.03 for $x = 0.0$, and -0.1 for $x = 0.1$ and 0.15. The obtained value of J_c^{res} decreases with the increase of La content, but its rate of reduction with x is faster than with H. This result indicates that doping of La acts as the effective weak link in reducing J_c^{res}.

At a constant magnetic field, the dissipation in the samples increases with the increase of doping. Figure 16 shows that dissipation is observed at $x = 0.25$ and 0.3 without applied magnetic field, as there is no Lorentz force. This behavior can be described within the AH theory. The granular samples have large number of junctions with different values of critical current J_c for each junction. When the applied current is higher than J_c for some junctions, the dissipation is observed. With the increase of current, the number of weaker junctions in the samples increases, and then the resistivity increases. The obtained results indicate that La doping is more effective in the dissipation than the applied magnetic field, as in the samples with larger amount of La, dissipation appears with no magnetic field.

Magnetization measurements

The magnetization of the superconducting state, M(μ_0H) of Gd(BaLa)123 with $x = 0.0$ and 0.1 have been measured at $T = 77$ K. Figure 17 shows the magnetization curves for these samples. The magnetization measurements allow determination of the first penetration field, as the field at which the deviation from linearity in the $M(H)$ dependence (Meissner state) begins, and second penetration field, as the field at which the curve shows a minimum with increase of H. The first and the second critical magnetic penetration fields, H_{c1}^{low} and H_{c1}^{high} are, respectively, the magnetic fields at which the magnetic flux begins to penetrate the superconducting intergrain and intragrain regions. The value of H_{c1}^{low} decreases from 150 G to 50 G and the value of H_{c1}^{high} decreases from 380 G to 160 G for $x = 0.0$ and 0.1, respectively. This result indicates that the critical values of penetration fields decrease, and the magnetic flux penetrates more easily into the sample upon La doping. The magnetism of the samples results from superposition of diamagnetism due to the Meissner effect and paramagnetism originating from the Gd ions. For magnetic fields less than H_{c1}^{low}, the magnetization has negative value, but with the increase of magnetic field, the magnetization of Gd ions increases and the total magnetization increases. At $x = 0.1$ the effect of Gd magnetic ions appears at low magnetic fields, and the magnetization increases to a positive value.

As can be seen in Figure 17, there is considerable hysteresis in $M(\mu_0 H)$ curves due to the large magnetic flux pinning. The hysteresis in the $M(\mu_0 H)$ curves at liquid nitrogen temperature with magnetic fields of about 2 T is still considerable. Therefore, the value of high critical magnetic field H_{c2} is much higher than 2 T at $T = 77$ K. The measurements of magnetization at the room temperature show that the samples in the normal state are paramagnetic.

The slope of the virgin magnetization curves for fields below H_{c1}^{low} represents the magnetic shielding effect. Comparison between the slopes of virgin magnetization curves for $x = 0.0$ and $x = 0.1$ samples indicates that the amount

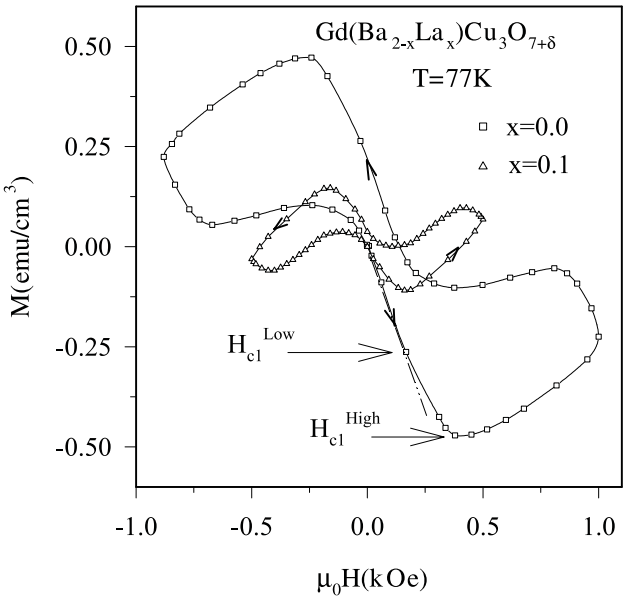

Fig. 17. Magnetic hysteresis loops of Gd(BaLa)123 for $x = 0.0$ and $x = 0.1$ at $T = 77$ K.

of 0.1 La decreases the shielding effect by about 28%. The slope of $M(H)$ curve for $H_{c1}^{low} < H < H_{c1}^{high}$ is less than the slope for $H < H_{c1}^{low}$, and is due to the penetration of magnetic field into the intergrain region. By comparing the differences between these slopes, we estimate the volume between the grains containing the intergrain material and voids to be about 36% and 47% for $x = 0.0$ and $x = 0.1$, respectively. As the mass density at $x = 0.0$ and $x = 0.1$ are, respectively, about 65% and 68% of the calculated values, we can estimate that the intergrain material contains about 3% for $x = 0.0$ and 22% for $x = 0.1$ of the total sample's mass. This indicates that for $x = 0.0$, the intergrain region practically consists of voids.

The hysteresis of $M(\mu_0 H)$ at a magnetic field due to the pinning effect decreases with La doping. The magnetic critical current density J_c^{mag} calculated by using the Bean theory [73] is higher than the obtained J_c^{res} from the resistivity measurements. This is reasonable as J_c^{mag} and J_c^{res} are related to the intragrain and intregrain superconducting behaviors, respectively. The value of J_c^{mag} decreases when the magnetic field increases from the value of H_{c1}. The maximum value of J_c^{mag}, which has been obtained from the magnetization at H_{c1}^{high} for $x = 0$ and 0.1 are 7.2×10^3 A/cm^2 and 4.8×10^3 A/cm^2 at $T = 77$ K, respectively.

Conclusion

We have studied the structural, electrical, and magnetic properties of the polycrystalline $Gd(Ba_{2-x}La_x)Cu_3O_{7+\delta}$ with $x \leq 0.8$. The Rietveld analysis of the XRD patterns shows that the crystal structure is isostructure 123 phase. At $x = 0.2$, the orthorhombic-tetragonal transition occurs. The resistivity of samples increases and T_c decreases with the increase of La doping. For $0.2 \leq x \leq 0.35$, there is a gradual insulating behavior in the normal state, while their behavior at the room temperature is metallic. The MIT and SIT occurs between $x = 0.35$ and $x = 0.4$. The dominant conduction mechanism is CG for $x \leq 0.35$, and VRH for $x \geq 0.4$. The decrease of T_c and increase of ρ_{300} upon La doping show a two-step behavior that could be the indication of existence of the two trap levels for holes. The study of magnetoresistance broadening indicates that the pinning energy decreases as a power-law with magnetic field. The power factor is about 0.5 for $x \leq 0.15$, and increases for $x \geq 0.2$. The coupling energy between the Josephson junctions decreases as H^{-n}; n is about 0.25 for $x \leq 0.15$, and increases for $x \geq 0.2$. It seems that a correlation exists between the magnetic properties in the superconducting transition and the normal state properties. Also, the pinning energy and coupling energy between the Josephson junctions decrease with the increase of La doping. This indicates that La ions act as weak links in the samples as is also indicated by the E-J results. The existence of the weak links related to La doping at the grain boundaries is again confirmed by the magnetization measurements. The critical penetration fields (H_{c1}^{low}, H_{c1}^{high}) and J_c^{mag} decrease with La doping.

We wish to thank M. Kariminezhad, H. Khosroabadi, P. Maleki, and Z. Mokhtari for technical assistance and useful discussions, and Drs. V. Daadmehr and M.R. Mohammadizadeh for useful discussions. This work was supported in part by the Offices of Vice President for Research and Dean of Graduate Studies at Sharif University of Technology.

References

1. M. Akhavan, Physica B **321**, 265 (2002)
2. M. Akhavan, Phys. Stat. Sol. (b) **241**, 1242 (2004)
3. A. Matsuda, K. Kinoshita, T. Ishii, H. Shibata, T. Watanabe, T. Yamada, Phys. Rev. B **38**, 2910 (1988)
4. A.P. Goncalves, I.C. Santos, E.B. Lopes, R.T. Henriques, M. Almeida, Phys. Rev. B **37**, 7476 (1988)
5. L. Sederholm, G.L. Goodman, J. Solid State Chem. **81**, 121 (1989)
6. J. Fink, N. Nucker, H. Romberg, M. Alexander, M.B. Maple, J.J. Neumeier, J.W. Allen, Phys. Rev. B **42**, 4823 (1990)
7. M.E. Lopez-Morales, D. Riso-Jara, J. Taguena, R. Escudero, S. La Placa, A. Bezing, V.Y. Leem E.M. Engler, P.M. Grant, Phys. Rev. B **41**, 6655 (1990)
8. A. Kebede, C.S. Jee, J. Schwelger, J.E. Crow, T. Mihalisin, G.H. Myer, R.E. Salomon, P. Schottmann, M.V. Kuric, S.H. Bloom, R.P. Guertin, Phys. Rev. B **40**, 4453 (1989)
9. Y. Wang, A. Manthiran, J.B. Goodenough, Physica C **161**, 574 (1989)
10. R. Fehrenbacher, T.M. Rice, Phys. Rev Lett. **70**, 3471 (1993)
11. Z. Zou, J. Ye, K. Oka, Y. Nishihara, Phys. Rev. Lett. **80**, 1074 (1998)
12. M.R. Mohammadizadeh, M. Akhavan, Phys. Rev. B. **68**, 104516 (2003)
13. S. Zhu, D.K. Christen, C.E. Klabunde, J.R. Thompson, E.C. Jones, R. Feenstra, D.H. Lowndes, D.P. Norton, Phys. Rev. B **46**, 5576 (1992)

14. T. Matsuura, H. Itozaki, Appl. Phys. Lett. **59**, 1236 (1991)
15. C.C. Chin, T. Morishita, Physica C **207**, 37 (1993)
16. M. Ye, J. Schroeder, M. Mehbod, R. Deltour, A.G.M. Jansen, P. Wyder, Physica C **258**, 95 (1996)
17. J. Schroeder, M. Ye, J.F. de Marneffe, M. Mehbod, R. Deltour, A.G.M. Jansen, P. Wyder, Physica C **278**, 113 (1997)
18. V. Daadmehr, M. Akhavan, Phys. Stat. Sol. (a) **193**, 153 (2003)
19. T.T.M. Palstra, B. Batlogg, R.B. van Dover, L.F. Schneemeyer, J.V. Waszczak, Phys. Rev. B **41**, 6621 (1990)
20. R.H. Koch, V. Foglietti, W.J. Gallagher G. Koren, A. Gupta, M.P.A. Fisher, Phys. Rev. Lett. **63**, 1511 (1989)
21. J.J. Kim, H. Lee, J. Chung, H.J. Shin, H.J. Lee, J.K. Ku, Phys. Rev. B **43**, 2962 (1991)
22. M.A. Dubson, S.T. Herbert, J.J. Calabrese, D.C. Harris, B.R. Patton, J.C. Garland, Phys. Rev. Lett. **60**, 1061 (1988)
23. A.C. Wright, K. Zhang, A. Erbil, Phys. Rev. B **44**, 863 (1991)
24. H. Iwasaki, O. Tanigichi, S. Kenmochi, N. Kobayashi, Physica B **196**, 2117 (1994)
25. T.T.M. Palstra, B. Batlogg, R.B. van Dover, L.F. Schneemeyer, J.V. Waszczak, Appl. Phys. Lett. **54**, 763 (1989)
26. B. Batlogg, T.T.M. Palstra, L.F. Schneemeyer, J.V. Waszczak, in: *Strong Correlation and Superconductivity*, edited by H. Fukyama, S. Maekawa, A.P. Malozemoff, Springer Series in Solid State Science, Vol. **89** (Springer-Verlag, Berlin, 1989)
27. A.P. Malozemoff, T.K. Worthington, E. Zeldov, N.C. Yeh, M.W. McElfresh, F. Holtzberg, in: *Strong Correlation and Superconductivity*, edited by H. Fukyama, S. Maekawa, A.P. Malozemoff, Springer Series in Solid State Science, Vol. **89** (Springer-Verlag, Berlin, 1989)
28. R. Griessen, Phys. Rev. Lett. **64**, 1674 (1990)
29. P.L. Gammel, L.F. Schneemeyer, J.V. Waszczak, D.J. Bishop, Phys. Rev. Lett. **61**, 1666 (1988)
30. V. Ambegaokar, B.I. Haplerin, Phys. Rev. Lett. **22**, 1364 (1969)
31. M. Tinkham, C.J. Lobb, in: *Solid State Physics*, edited by H. Ahrenreich, D. Turnbull (Academic, New York, 1989), Vol. **42**, p. 91
32. M. Tinkham, Phys. Rev. Lett. **61**, 1658 (1988)
33. M. Mohammadizadeh, M. Akhavan, Physica C **30**, 134 (2003)
34. M.R. Mohammadizadeh, M. Akhavan, Supercond. Sci. Technol. **16**, 538 (2003)
35. M. Mirzadeh, M. Akhavan, submitted to Supercond. Sci. Technol. (2004)
36. M. Simeckova, P. Kiko, Physica C **179**, 253 (1991), and refrences therein
37. S. Li, E.A. Hayri, K.V. Ramanujachary, M. Greenblatt, Phys. Rev. B **38**, 2450 (1988)
38. J.B. Goodenough, J.M. Lango, L.B. Tabelleu, New Series, Vol. III/4a (Springer-Verlag, Berlin, 1970)
39. CRD *Handbook of Chemistry and Physics*, 75th, edited by D.A. Lide, H.P.R. Frederikee (CRC Press, FL, 1995)
40. W.H. Tang, J. Gao, Physica C **298**, 66 (1998)
41. R.J. Cava, Bibatbogg, R.M. Fleming, S.A. Sunshine, A. Ramire, Phys. Rev. B **37**, 5912 (1988)
42. M.R. Mohammadizadeh, M. Akhavan, Eur. Phys. J. B **33**, 381 (2003)
43. C. Quitmsnn, D. Andrich, C. Jarchow, M. Fleuster, B. Beschoten, G. Guntherodt, V.V. Moshchalkov, G. Mante, R. Manzke, Phys. Rev. B **46**, 11813 (1992)
44. B.I. Shklovskii, A.L. Efros, *Electronic Properties of Doped Semiconductors*, edited by M. Cardona, P. Fulde, H.-J. Queisser, Springer Series in Solid State Sciences, Vol. 45 (Springer-Verlag, Berlin, 1984)
45. A.L. Efros, B.I. Shklovskii, J. Phys. C **8**, L49 (1975)
46. N.F. Mott, E.A. Davis, *Electronic Processes in Non-crystalline Materials*, 2nd edn. (Clarendon, Oxford, 1979)
47. Z. Yamani, M. Akhavan, Solid State Commun. **107**, 197 (1998)
48. W.H. Tang, J. Gao, Physica C **315**, 66 (1999)
49. M. Mokhtari, H. Khosroabadi, M. Akhavan, Phys. Stat. Sol. (c) **1**, 1891 (2004)
50. R.J. Cava, A.W. Hewat, E.A. Hewat, B. Batlogg, M. Marezio, K.M. Rabe, J.J. Krajawski, W.F. Peck, Jr., L.W. Rupp, Jr., Physica C **165**, 419 (1990)
51. H.S. Gamchi, G.J. Russell, K.N.R. Taylor, Phys. Rev. B **50**, 12950 (1994)
52. D.H. Kim, K.E. Gray, R.T. Kampwirth, D.M. McKay, Phys. Rev. B **42**, 6249 (1990)
53. C. Gaffney, H. Petersen, R. Bednar, Phys. Rev. B **48**, 3388 (1993)
54. H. Shakeripour, M. Akhavan, Supercond. Sci. Technol. **14**, 234 (2001)
55. W. Chen, J.P. Franck, J. Jung, Physica C **341-348**, 1195 (2000)
56. M. Kariminezhad, H. Khosroabadi, M. Akhavan, Phys. Stat. Sol. (c) **1**, 1855 (2004)
57. P. Maleki, H. Khosroabadi, M. Akhavan, Phys. Stat. Sol. (c) **1**, 1871 (2004)
58. B.W. Kang, W.N. Kang, S.H. Yum, J.Z. Wu, Phys. Rev. B **56**, 7862 (1997)
59. M. Mirzadeh, H. Khosroabadi, M. Akhavan, Phys. Stat. Sol. (c) **1**, 1875 (2004)
60. M. Tinkham, *Introduction to Superconductivity* (McGraw-Hill Press, New York, 1975)
61. Y. Yeshurum, A.P, Malozamoff, Phys. Rev. Lett. **60**, 2201 (1988)
62. H.E. Horng, H.H. Sung, B.C. Yao, H.C. Yang, Physica C **185-189**, 2221 (1991)
63. G. Deutscher, K.A. Muller, Phys. Rev. Lett. **59**, 1745 (1987)
64. R. Gross, P. Chaudhari, D. Dimos, A. Gupta, G. Koren, Phys. Rev. Lett. **64**, 228 (1990)
65. D.H. Kim, K.E. Gray, R.T. Kampwirth, K.C. Woo, D.M. McKay, J. Stein, Phys. Rev. B **41**, 11642 (1990)
66. Z.H. Wang, X.W. Cao, Solid State Commun. **109**, 709 (1999)
67. L.M. Paulius, C.C. Almasan, M.B. Maple, Phys. Rev. B **47**, 11627 (1993)
68. Z.H. Wang, S.Y. Ding, Physica C **341-348**, 1247 (2000)
69. H. Khosroabadi, V. Daadmehr, M. Akhavan, Physica C **384**, 169 (2003)
70. P.W. Anderson, Phys. Rev. Lett. **9**, 309 (1962)
71. J.D. Hettinger, A.G. Swanson, W.J. Skocpol, J.S. Brooks, J.M. Graybeal, P.M. Mankiewich, R.E. Howard, B.L. Straughn, E.G. Burkhardt, Phys. Rev. Lett. **62**, 2044 (1989)
72. E. Zeldov. N.M. Amer, G. Koren, A. Gupta, R.J. Gambino, M.W. Mc Elfresh, Phys. Rev. Lett. **62**, 3093 (1989)
73. C.P. Bean, Rev. Mod. Phys. **36**, 31 (1964)